Restoration of Images Affected by Welding Fume

Edwilson Vaz-Jr
Federal University of
Rio Grande
Center for Computational Science - C3
Rio Grande, Brazil
Email: edwilson@furg.br

Paulo Drews-Jr
Federal University of
Rio Grande
Center for Computational Science - C3
Rio Grande, Brazil
Email: paulodrews@furg.br

Cristiano Steffens
Federal University of
Rio Grande
Center for Computational Science - C3
Rio Grande, Brazil
Email: cristianosteffens@furg.br

***Abstract*—Machine vision performs an important role in many applications, including robotics. Combined with classical instrumentation, welding robots can use a camera to perceive the scene and take a decision. A camera attached to the robot body and machine vision system work as the eyes of the robot during the welding process. However, image-based systems are susceptible to the interference of fumes, sparks, dust, and artifacts generated as a side effect of the welding process. Fume can adhere to the lenses and degrades the image, introducing a negative impact on the processing pipeline. This paper proposes a novel image fusion based algorithm that minimizes the effects caused by the fume adhered to the camera lens. Results show the proposed method is able to enhance the overall image quality, outperforming classical alternatives for similar problems.**

I. Introduction

Automated welding robots have become commonplace in modern manufacturing since the arc welding process produces non-ionizing radiation, sparks, and fume that makes the environment hazardous and unhealthy. Normally, there is a camera next to these robots which is responsible to perceive the robot's surrounding and enable it to take decision [1].

The camera is usually positioned near to the welding torch [2]–[4] being susceptible to the effects of welding waste. Since camera lenses are expensive and they can easily damage, lenses are protected by disposable glasses. However, the welding process can last hours to complete and the change of the glasses cannot be done anytime because it needs to be manually done. Furthermore, welding flow needs to be interrupted to be possible the change of the glasses. This interruption can damage the welding quality, thus the operator is only able to replace the disposable glass after the end of the welding process [5].

The adhered waste in the glass causes distortion in the captured image. Thus, an effective method to improve the image is mandatory for this task. Fig. 1 shows an example of a welding robot and illustrates the proximity between the camera and the welding torch. This example shows a Bug-O Matic Weaver - a remotely operated robotic system manufactured by the Bug-O Systems.

Image degradation due to welding depends on factors such as focal distance, camera aperture, environmental lightning, and others. Welding produces bright light, spatter welding, sparks, and fume that distort the captured light by the camera sensor [6]. In our experimental evaluation, we found fume is the most important degradation factor since we can deal with the sparks using specialized hardware, as an industrial vacuum cleaner, and the bright light can be minimized using an appropriate camera aperture. Fig. 1) shows an industrial vacuum cleaner system attached to the welding torch. Beside the already expressed annotations in the image, a vacuum cleaner is attached with the welding torch and disposable glasses are in front of the camera lenses, inside the metallic cylinder. In this work, we focus on welding fume adhered to the disposable glass or to camera lenses. Adhered fume reduces contrast, brightness and distorts the image color [7].

Although the occurrence of spatters is frequent during the welding process, an empirical evaluation has shown spatter has a minor impact in terms of image content and can be significantly reduced with proper mechanical shielding. Spatters adherents to the lenses affect just regions of the image where they protrude in the lenses. Even though spatters generate some distortion in the image, this problem is not as impactful as fume. Spatters do not distort the entire image and, comparatively with fume, produce effects almost invisible to human eye. A comparison between the implications of each phenomenon is shown in Fig. 2. Image affected by welding spatter is similar to the image acquired using a clean disposable glass. However, fume adhered to the glass corrupts the image quality.

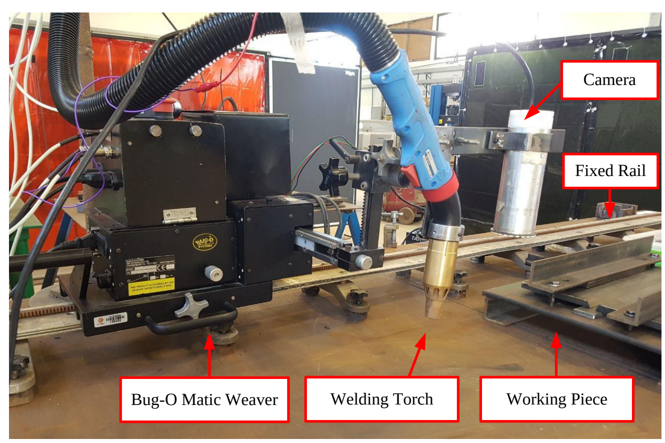

Fig. 1. An example of a welding robot and its specific parts. The proximity between the camera and the welding torch is common in vision-based system such as Bug-O Matic system presented in the figure.

Once images captured by the camera are distorted, image processing algorithms can misunderstand the scene in which the welding robot is acting in and then may take a wrong

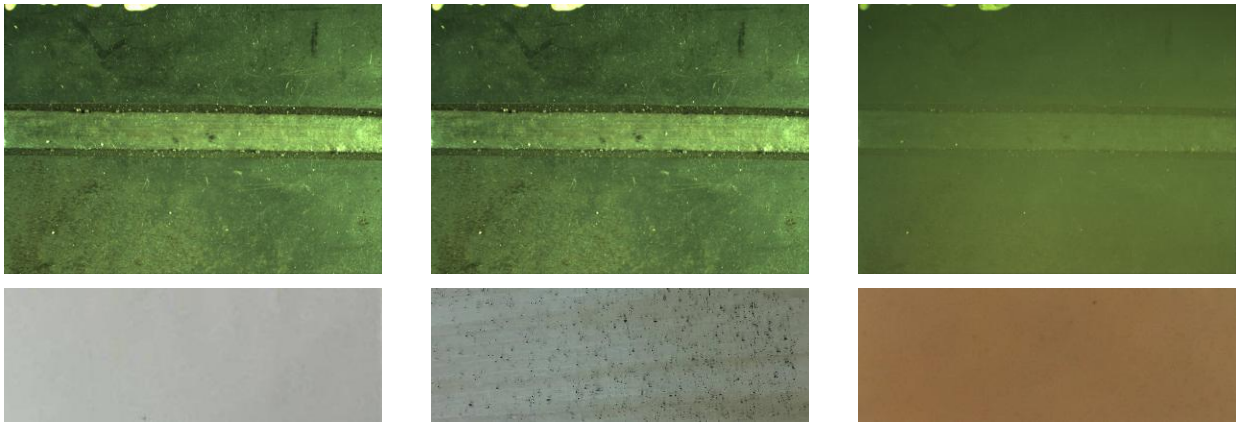

(a) (b) (c)

Fig. 2. Example of images captured using disposable glasses affected by welding spatter and fume in front of the camera lens: (a) clean disposable glass, (b) disposable glass affected by welding spatter, (c) disposable glass affected by fume. Captured images are presented in the top while images of each disposable glass are presented in the bottom. The images were captured during an off-line experiment.

decision making to the welding process. Fume simultaneously with welding spatters cause sharpness loss, loss of contrast, color shifting and visual anomalies that insert fake elements in the image. Previously cited effects affect directly the systems based on computer vision. Furthermore, they represent a challenge for the effective application in the real world. Assuming fume causes most of these effects and occurs approximately homogeneous in the lenses, previous works [8]–[11] does not deal properly with all of these issues.

This work is focused on restore image affected by welding fume adhered to camera lenses (or disposable glasses). Spatter, as seen before, is not hazardous to the computer vision algorithms. Smoke problem is not covered in this work as the robot system, once the camera does not look directly to the welding torch, but a step in front of it, making possible it's decision making before welding. Welding fume occurs independently of smoke occurrence. Welding fume is in the air of the shop floor and any welding process is prone to generate it. Thus, with or without smoke and spatter, welding fume is, in fact, a problem in automatic robotic welding and our goal is to recover the image as close as possible to the real scene.

Contributions: Our work aims to suppress undesired image artifacts generated when welding fume adheres to the camera lenses. The main contribution is an algorithm based on Image Fusion that restores the original information of the scene. This algorithm stands on the use of several image processing methods and selects the best of these methods to restore the image. The proposed method is compared with other image processing methods and quantified through image quality assessment methods such as MSSIM [12], FSIMc [13], and PSNR [14]. Another contribution is a welding fume dataset, which presents the ground truth for each image affected by welding fume.

II. RELATED WORK

We did not find any work trying to solve or minimize the fume adhered to the camera lens according to the best of our knowledge. Therefore, we take into consideration papers which approach similar problems. In [9], [10], [15], authors proposed methods to remove dust particles in the camera lenses. In all three cases, authors try to create a model to find dust related artifacts, i.e. projections of the dirt adherent to the camera lenses in the image plane. Dust and welding fume present similarities, however, its shape and the way to adhere the camera lens is distinct. The previous work assumes dust adheres in a certain location in the lenses whereas the welding fume presents a homogeneous behavior. This difference results in a distinct way to recover the information: dust need to be identified, removed and its neighborhood utilized for the reconstruction of the image. Nonetheless, fume affects the image in an approximately homogeneous way. Furthermore, dust can block the light to travel through while the fume usually is translucent.

In [8], [16]–[18], authors present methods to deal with thin occluders, object and fence removal, which perceive patterns and minimize the effects caused by the present occluder. The main difference between these occluders and welding fume is fume spreads directly in camera lenses, preventing light from the scene propagates in the sensor. However, occluders are generally objects which have not adhered to the lenses but are obstructing the scene somehow. Occluders are usually detected by changing some parameters of the camera and take multiple images of the same or complementary scene. This method is impossible to be adopted here since the restoration needs to happen during to welding process. Thus, parameters of the camera can not be changed, images are usually taken sequentially and it is required real-time performance. These facts limit the applicability of these works on thin occluders.

Others works propose methods to the problem of raindrops adherent to camera lenses or a close surface [11], [19]–[21]. They recognize raindrop by optical flow (in a video) and its shape or intensity change in the image, for example. After recognizing raindrops, these methods can restore the content whether some information inside it can be used, or use interpolation technique to fill out the missing data [22]. Raindrop approach differs from welding fume problem in terms of behavior. Raindrops influence a region of the image and allow the light to pass through the sensor, although generates a blur effect. The method uses the movement of the raindrop in several images, which in welding fume, as previously expressed, is not viable.

Image fusion is a technique that combines various image processing methods with the intent to return a better image than the source one. This method shows impressive results, mainly when the scene is being corrupted in a homogeneous way. Furthermore, image fusion techniques have been adopted to restore images affected by participating media. In [23], the image fusion based method deals with the problem of underwater images. Water interferes in the captured image causing loss of color and contrast. Authors also adopted image fusion to deal with haze [24] and decolorized images [25]. As we can see, image fusion is a general tool that can be adapted to improve the image affected by welding fume.

III. IMAGE FUSION

Once welding fume adhered to the camera lenses causes an effect of blurring and color losing, we noticed a single classical image processing method would not minimize all effects caused by the fume. Therefore, image fusion is a prominent technique for the restoration problem. This method allows us to use several image processing methods and generates a better output than using each method individually. Image fusion is based on mixing image processing filters, called **input images**, and their respective **weight maps**. Therefore, image fusion stands on a source image affected by welding fume and fuses the results of various image processing filters and their respective weight maps to obtain the final result.

Weights maps select the best of each input pixel to compose the final result, working as a filter. Besides that, weight maps are normalized from 0 to 1 for each input image in order to ensure that the sum of each pixel (x, y) for all weight maps is equal to one. Thus, normalization keeps each pixel value of the resulting image within the color representation. On the other hand, inputs combine classical image processing techniques that, in theory, recover the image from the effects generated by the fume. In our case, the effects are mainly color loss and high-frequency details. Equation (1) is a pixel to pixel multiplication and represents the naive version of the image fusion, using just the original scale of image [26].

$$R_N(x,y) = \sum_{k=1}^{K} I_k(x,y) W_k(x,y), \quad (1)$$

where K is the number of input images, R_N represents the result obtained by the naive fusion, I_k is the input image with index k and W_k is the weight map associated to the input image with the same index. However, a multi-scale approach is assumed by obtaining a final result more realistic and more detailed than naive approach. This approach intends to obtain results that minimize the effects of the fume making the image more suitable to be processed by computer vision algorithms, e.g. [1], [27]. The scales are based in the Gaussian Pyramid where both inputs and weight maps are downsampled. Fusion is computed and the result is upsampled to the original size (of the source image). Upsampling to original size is a fundamental procedure since the model induces a sum of all images in all calculated scales, which is only possible if all images have the same size. Equation (2) shows the operation performed by the fusion algorithm.

$$R_{MS}(x,y) = \sum_{l=1}^{l_{max}} \sum_{k=1}^{K} L\{I_k(x,y)\} G\{W_k(x,y)\}, \quad (2)$$

where R_{MS} corresponds to the result generated by the algorithm with a multi-scale approach. $G\{W_k(x,y)\}$ is the Gaussian Pyramid of weight maps and $L\{I_k(x,y)\}$ is the Laplacian Pyramid of input images. The term l represents the levels of the Gaussian Pyramid and l_{max} is the maximum level of the Pyramid. The term I_k is the input image with index k and W_k is its respective normalized weight map of the input image. K represents the number of input images. We illustrate the set of operations done by the fusion algorithm in Fig. 3. It is important to highlight that the source image is not the same as input image of the method [23]. Input images are estimated based on image processing techniques as detailed in the next section and source image is the one affected by welding fume.

A. Input images

Once it is known which degradation welding fume produces in the image, inputs of the image fusion algorithm can be estimated to minimize these effects. We notice the most important effects caused by welding fume in an image are lose of color and blur. We adopted two input images to supply these needs: white balance and contrast enhancement. White balance intents to help in correcting the color lost by the incidence of fume and contrast enhancement is adopted to enhance high frequencies of the image.

The *first input image* is achieved using white balance. We adopted the Grey-World algorithm [28], which tends to equalize the three color channels in the RGB color space in order to make a redistribution of pixel values. This equalization restores colors, which are generally lost in the images affected by welding fume adhered to the lens or disposable glass.

The *second input image* is named contrast enhancement. The idea is to expand the general contrast of the image affected by fume. This input image also relies on the Grey-World assumption to correct colors as the first one. However, we also apply a Local Adaptive Histogram Equalization (CLAHE) [29] to obtain a uniform distribution of pixels between representation values. Histogram Equalization generates an effect of contrast enhancement in an effective way.

B. Weight Maps

Weight maps are grayscale images based on the source image whose the main function is selecting the best of each inputs to compose the final image. These maps are not based on a learning technique. They are application-driven images to define the importance of each pixel of the input images. In other terms, weight maps filter and generate a value from $[0;1]$ for each pixel with the intent to weight higher values to the most important pixels, influencing the resulting image.

Weight maps select which region of the image must receive more attention to compose the final image. Generated weight maps are normalized among them, creating just one weight map for each input image. The normalization of the weight maps follows the Equation (3). The intention with normalization is based on avoiding that any pixel exceeds the color

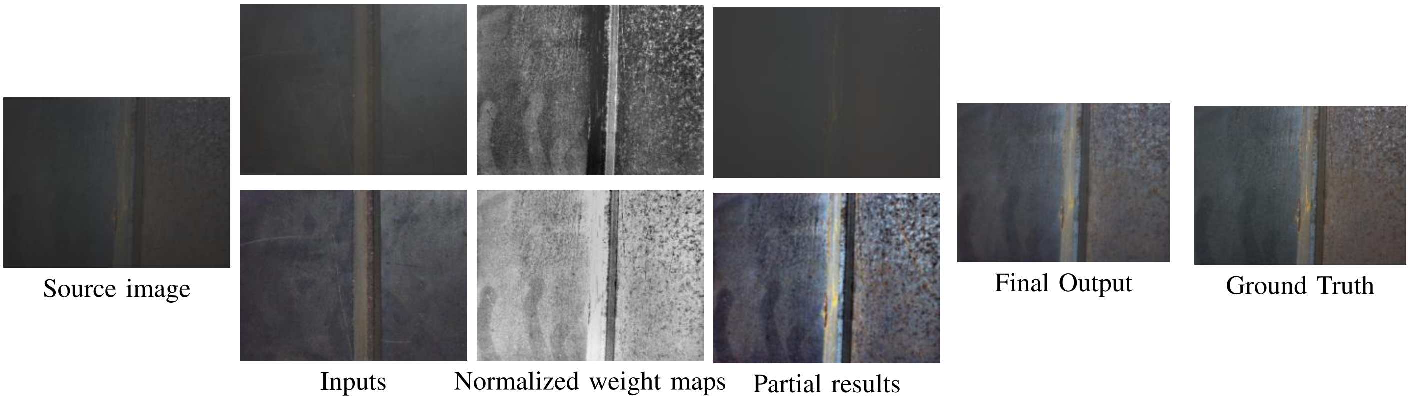

Fig. 3. The proposed image fusion pipeline using a sample image. The first column shows the source image affected by the fume. The second column shows the called input images, where the top image is the white-balanced image and the bottom image is the contrast enhancement. The third column shows the corresponding normalized weight maps for each input. The fourth column shows the partial results obtained by the dot product of the inputs and normalized weight maps. Finally, the last two columns show respectively the result of proposed fusion scheme and the ground truth of the source image (acquired with a glass with no fume incidence in front of the camera lens).

representation maximum value in the output image, then the sum of all weight maps must be equals one.

$$W_k = \sum_{n=1}^{N} \frac{O_n}{\sum_{t=1}^{T} A_t}, \tag{3}$$

where W_k is the normalized weight map to the input image with index k, N is the number of weight maps for only one input image and T is the total number of weight maps for all input images. A represents the sum of all weight maps for all input images and O expresses the sum of all weight maps for one specific input image (with the k-th index).

In this work, we use two different weight maps. The first is called *local contrast weight map*. We adopt this weight map because of its capacity of keeping contrast in small regions of the image. This map is fundamental to the contrast enhancement input image, once it keeps regions where the input image filter effectively acted. Equation (4) shows the local contrast weight estimation:

$$W_{LC} = ||I^k - I^k_{\omega hc}||, \tag{4}$$

where I^k is the luminance of the input image with index k and $I^k_{\omega hc}$ indicates the smoothed version of the luminance of the same image. We adopted a Gaussian Filter with kernel size 5×5 to obtain the smoothed image.

Second weight map is called *exposition weight map* [30]. This map evaluates the exposition of each pixel, indicating which pixels present greater relevance for each input image. This weight map intermediates the preservation of local contrast weight map keeping a constant appearance. Equation (5) represents this weight map:

$$W_E = e^{\left(-\frac{(I^k(x,y)-0.5)^2}{2\sigma^2}\right)}, \tag{5}$$

where $I^k(x,y)$ is the pixel in the (x,y) position of the input image in the k-th index, 0.5 is the most usual value to a normalized pixel be well exposed. σ represents the standard deviation and e is the exponential factor. Briefly, exposition weight map provides higher values to pixels next to extreme values, i.e. 0 and 1. Furthermore, intermediaries values are penalized.

IV. RESULTS AND DISCUSSION

The experimental evaluation of the results obtained is achieved using three image quality measures: Multiscale Structural Similarity index (MSSIM) [12], Feature Similarity index (FSIM) [13] and Peak Signal-to-Noise Ratio (PSNR) [14]. MSSIM is a multi-scale version of the full-reference metric SSIM [31] which utilizes a reference image (ground truth) to compare the similarity with the obtained result based on average and variance of the pixels. MSSIM provides a quantitative metric using a decimal value between -1 and 1. This metric compares similarity in the structures of both images and evaluates how close they are, once higher values in the metric, closer the images are. The second adopted metric is called FSIM [13]. FSIM also evaluates the method in comparison with the ground truth, but it uses other characteristics from the image based on the human perception. Similarly to MSSIM metric, higher values in FSIM indicates ground truth is close to the evaluated method. In this work, we adopted the FSIMc version [13] which is capable to identify the similarity considering all three channels of color.

PSNR is a metric which measures the ratio between the signal of an image and its respective noise. This metric is fundamental to prove the proposed method does not generate as much noise as the classical image processing methods. PSNR generates a value according to the details of the image, which higher the value, better the signal-to-noise ratio.

We compared our method against classical image processing methods that can deal with the problem generated by welding fume. Algorithms evaluated are Global Histogram Equalization and Local Adaptive Histogram Equalization [29], this last one using its amplitude as 5. Besides that, we created an **welding fume dataset** with 42 images, of which 21 are affected by welding fume and 21 correspond to their respectively ground truths. We used three disposable glasses with different levels of adhered welding fume to make sure the evaluation is fair enough, as shown in Fig. 6. Ground truth images were captured using the glass presented in Fig. 6-(a)

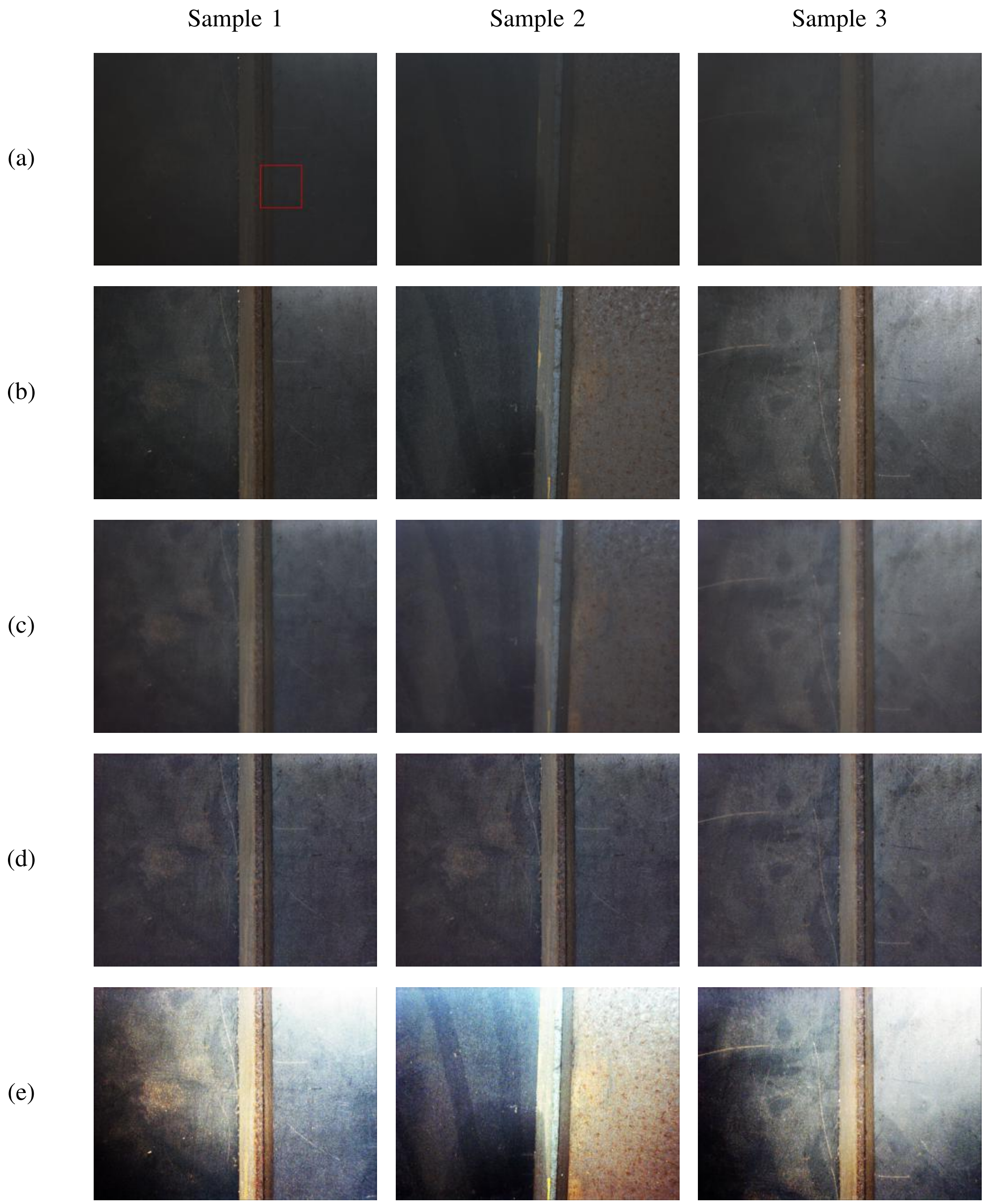

Fig. 4. Qualitative results between three different sample images affected by welding. The first column represents Sample 1, second column represents Sample 2 and third column represents Sample 3. In each row: (a) image affected by welding fume, (b) its corresponding ground truth (i.e. new disposable glass in front of the lens), (c) proposed method, (d) CLAHE, (e) Global Histogram Equalization. In (a), the red squared area shows the highlighted region of the image shown in Fig. 5.

and the other three glasses were utilized to capture images affected by welding fume. These glasses were obtained in welding process using a real robot. No images are altered or generated artificially in this dataset. The **welding fume dataset** is publicly available at `http://paulo.c3.furg.br`.

Table IV shows the quantitative results on our welding fume dataset. Table IV express the results with the mean values and their respective standard deviation. Assuming MSSIM metric, the proposed method obtained higher values than the other compared methods for all images of the dataset, presenting a higher average value between the methods. The main explanation for this difference between the proposed method and classic methods is other methods are not able to correct the chromatic of the image. However, the redistribution of pixel values sometimes generates the visual perception sensation of correction of the image colors. Fig. 4 visually illustrates the results presented by the three methods in three sample images.

The proposed method was not the best method in only two cases assuming FSIMc metric. Furthermore, the difference between the three methods was not as high as in the MSSIM metric in most of the cases. The preference by saturated images is a typical behavior of the human perception that is not reasonable for computer vision algorithms [24] and FSIMc evaluates characteristics visually plausible to the human

Fig. 5. Zooming in a small area of the Sample 1 image shown in Fig. 4-(a) highlighted by a red square. Besides Fig. 4-(a), we zoom all other images of Sample 1 in the same region. These images aim to highlight the noise caused by the classical methods and the proposed one, and though a comparison between all methods with the ground truth and source image. From left to right: (a) Image affected by welding fume, (b) Ground truth, (c) Proposed method, (d) CLAHE, (e) Global Histogram Equalization.

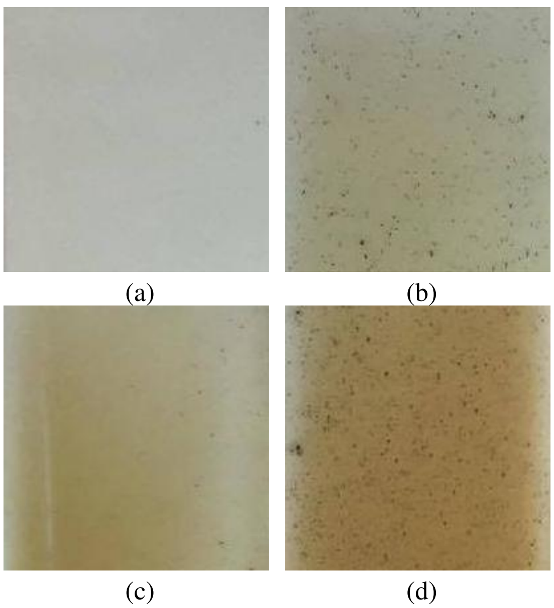

Fig. 6. Disposable glasses obtained in welding tests. They are adopted to create the welding fume dataset. Figure (a) presents the glass utilized to generate the ground truth images. Figures (b), (c) and (d) show the three glasses affected by welding fume utilized to create the welding fume dataset.

perception. Although the proposed method did not obtain higher values in all images for this metric, it presents a larger average with limited standard deviation. Fig. 4 visually illustrates the results presented by the methods and Fig. 5 presents a zooming in a small region of the images shown in Fig. 4. The region is highlighted by a red squared area in Fig. 4-(a).

Results in Table IV show the proposed method obtains the largest mean against the other methods. Histogram Equalization obtains low intensity comparing to the other methods as expected. Histogram Equalization due to the global approach brings a lot of high frequencies to the image and level up pixels which are not important. Local Histogram Equalization achieves better results compared to its global approach. This is justified by its own characteristic: it acts in locally, in small areas, presenting higher frequencies to the image and generating a lot less noise. As already introduced, the proposed method gathers better results and this is explained by the fusion of techniques. The combination of several image processing filters and the application of Gaussian Pyramids induce to a noiseless image without losing edges.

Presented results evaluate the proposed method in comparison to image processing techniques. Usual image processing techniques do not have the capacity to improve all lost characteristics by fume. MSSIM and FSIMc proved that, in comparison to the ground truth, the proposed method presents better results than others in terms of structure, color, and human perception. PSNR shows the proposed method does not increase noise in contrast with classical methods. This aspect is fundamental to computer vision algorithms once noisy images are generally difficult to recognize patterns and identify lines. Thus, noisy images can easily trick computer vision algorithm that misunderstand the observed scene.

TABLE I. RESULTS OF THE METRICS MSSIM, FSIMC AND PSNR. THE RESULTS ARE EXPRESSED AS: (MEAN, STANDARD DEVIATION). THE BEST RESULTS ARE HIGHLIGHTED USING BOLD LETTERS.

Method/metric	MSSIM	FSIMc	PSNR
Proposed method	(**0.7956, 0.0714**)	(**0.9607, 0.0171**)	(**24.2057, 3.2572**)
CLAHE	(0.5103, 0.0323)	(0.9234, 0.0587)	(21.3854, 1,8937)
Histogram Equal.	(0.2895, 0.0684)	(0.7482, 0.05154)	(9.4481, 0.8277)

V. CONCLUSION

This work proposes a method for the problem of images affected by fume during an automated welding process. The proposed method obtains higher values in the evaluated metrics: MSSIM, FSIMc, and PSNR. These metrics are image quality analysis metrics that evaluate in distinct ways how close the resulting image of a method is from the ground truth, and the ratio between signal and noise in the images. To the best of our knowledge, this work is the first to approach this problem which is frequent in automated welding robots. Once the welding process can spend more than an hour, fume increases and the process should not stop to the camera lenses or the disposable glasses be changed or cleaned.

Future work will be focused on the use of learning-based approaches such as Convolutional Neural Networks to improve the image quality. Furthermore, we also plan to expand our dataset to cover a larger number of conditions including several illuminations, camera resolution, and fumes level. This larger dataset is crucial to train Convolutional Neural Networks too.

Besides welding fume, future work will apply the same method here present to other applications and fields.

Acknowledgment

The authors would like to thank to CAPES/CNPq and FAPERGS for the financial support to develop this research. Also thanks to LaPeS/FURG Welding Research Laboratory and NAUTEC/FURG Intelligent Automation and Robotics Laboratory, for their support in the operationalization of the present research.

References

[1] A. Weis, J. Mor, L. Soares, C. R. Steffens, P. Drews-Jr, M. Faria, P. Evald, R. Azzolin, N. D. Filho, and S. Botelho, "Automated seam tracking system based on passive monocular vision for automated linear robotic welding process," in *IEEE International Conference on Industrial Informatics*, 2017, pp. 305–310.

[2] M. Kawahara, "Tracking control system using image sensor for arc welding," *Automatica*, vol. 19, no. 4, pp. 357–363, 1983.

[3] P. Drews, B. Frassek, and K. Willms, "Optical sensor systems for automated arc welding," *Robotics*, vol. 2, no. 1, pp. 31–43, 1986.

[4] L. Zhang, W. Ke, Q. Ye, and J. Jiao, "A novel laser vision sensor for weld line detection on wall-climbing robot," *Optics & Laser Technology*, vol. 60, pp. 69–79, 2014.

[5] L. B. Soares, A. Weis, R. N. Rodrigues, P. L. J. Drews-Jr, B. Guterres, S. S. C. Botelho, and N. D. Filho, "Seam tracking and welding bead geometry analysis for autonomous welding robot," in *IEEE Latin American Robotics Symposium (LARS) and Brazilian Symposium on Robotics (SBR)*, 2017, pp. 1–6.

[6] K. Hang and G. Pritschow, "Reducing distortions caused by the welding arc in a laser stripe sensor system for automated seam tracking," in *IEEE International Symposium on Industrial Electronics (ISIE)*, 1999, pp. 919–924.

[7] N. T. Jenkins and T. W. Eager, "Chemical analysis of welding fume particles," *Welding Journal*, vol. 84, pp. 87–93, 2015.

[8] J. Gu, R. Ramamoorthi, P. Belhumeur, and S. Nayar, "Removing image artifacts due to dirty camera lenses and thin occluders," *International Conference on Computer Graphics and Interactive Techniques Asia (ACM SIGGRAPH)*, 2009.

[9] C. Zhou and S. Lin, "Removal of image artifacts due to sensor dust," *IEEE Conference of Computer Vision and Pattern Recognition (CVPR)*, 2007.

[10] P. Yang, L. Chen, J. Tian, and X. Xu, "Dust particle detection in surveillance video using salient visual descriptors," *Computers and Electrical Engineering*, 2016.

[11] D. Eigen, D. Krishnan, and R. Fergus, "Restoring an image taken through a window covered with dirt or rain," *IEEE International Conference on Computer Vision (ICCV)*, 2013.

[12] Z. Wang, E. Simoncelli, and A. Bovik, "Multi-scale structural similarity for image quality assessment," *Asilomar Conference on Signals, Systems and Computers (ACSSC)*, vol. 2, pp. 1398–1402, 2004.

[13] L. Zhang, L. Zhang, X. Mou, and D. Zhang, "Fsim: A feature similarity index for image quality assessment," *IEEE Transactions on Image Processing*, vol. 20, no. 8, pp. 2378–2386, 2011.

[14] Z. Wang and A. C. Bovik, "A universal image quality index," *IEEE Signal Processing Letters*, vol. 9, no. 3, pp. 81–84, 2002.

[15] C. Li, K. Zhou, and S. Lin, "Removal of dust artifacts in focal stack image sequences," *IEEE International Conference on Pattern Recognition (ICPR)*, 2012.

[16] A. Yamashita, A. Matsui, and T. Kaneko, "Fence removal from multifocus images," *International Conference on Pattern Recognition (ICPR)*, 2010.

[17] S. McCloskey, M. Langer, and K. Siddiqi, "Removing partial occlusion from blurred thin occluders," *International Conference on Pattern Recognition (ICPR)*, 2010.

[18] C. Negi, K. Mandal, R. Sahay, and M. Kankanhalli, "Super-resolution de-fencing: Simultaneous fence removal and high-resolution image recovery using videos," *IEEE International Conference on Multimedia and Expo Workshops (ICMEW)*, 2014.

[19] S. You, R. T. Tan, R. Kawakami, Y. Makaigawa, and K. Ikeuchi, "Adherent raindrop modeling, detection and removal in video," *IEEE Transactions on Pattern Analysis and Machine Intelligence (TPAMI)*, vol. 38, no. 9, pp. 1721–1733, 2016.

[20] S. You, R. Tan, R. Kawakami, Y. Makaigawa, and K. Ikeuchi, "Raindrop detection and removal from long range trajectories," *Asian Conference on Computer Vision (ACCV)*, 2014.

[21] Q. Wu, W. Zhang, and B. Vijaya Kumar, "Raindrop detection and removal using salient visual features," *IEEE International Conference on Image Processing (ICIP)*, 2012.

[22] M. Bertalmio, G. Sapiro, V. Caselles, and C. Ballester, "Image inpainting," *International Conference on Computer Graphics and Interactive Techniques (SIGGRAPH)*, pp. 417–424, 2000.

[23] C. Ancuti, C. O. Ancuti, T. Haber, and P. Bekaert, "Enhancing underwater images and videos by fusion," *IEEE Conference of Computer Vision and Pattern Recognition (CVPR)*, pp. 81–88, 2012.

[24] C. Ancuti and C. O. Ancuti, "Single image dehazing by multi-scale fusion," *IEEE Transactions on Image Processing*, vol. 22, no. 8, pp. 3271–3282, 2013.

[25] C. O. Ancuti, C. Ancuti, and P. Bekaert, "Decolorizing images for robust matching," *IEEE International Conference on Image Processing (ICIP)*, pp. 149–152, 2010.

[26] C. O. Ancuti, C. Ancuti, C. D. Vleeschouwer, and A. C. Bovik, "Single-scale fusion: An effective approach to merging images," *IEEE Transactions on Image Processing*, vol. 26, no. 1, pp. 65–78, Jan 2017.

[27] B. Q. Leonardo, C. R. Steffens, S. C. da Silva Filho, J. L. Mr, V. Huttner, E. Leivas, V. S. da Rosa, and S. S. C. Botelho, "Vision-based system for welding groove measurements for robotic welding applications," in *IEEE International Conference on Robotics and Automation (ICRA)*, May 2016, pp. 5650–5655.

[28] M. Ebner, "Color constancy," *Wiley 1st Edition*, 2007.

[29] K. Zuiderveld, "Contrast limited adaptive histogram equalization," *Graphic Gems IV San Diego: Academic Press Professional*, p. 474485, 1994.

[30] T. Mertens, J. Kautz, and F. Van Reeth, "Exposure fusion," *Pacific Conference on Computer Graphics and Applications*, 2007.

[31] Z. Wang, A. Bovik, H. Sheikh, and E. Simoncelli, "Image quality assessment: From error visibility to structural similarity," *IEEE Transactions on Image Processing*, vol. 13, no. 4, pp. 600–612, 2004.